Colloids and Surfaces B: Biointerfaces 160 (2017) 254–264

Contents lists available at ScienceDirect

Colloids and Surfaces B: Biointerfaces

journal homepage: www.elsevier.com/locate/colsurfb

Full length article

Gold nanoconjugates reinforce the potency of conjugated cisplatin and doxorubicin

Sana Iram[a], Manaal Zahera[a], Salman Khan[a], Imran Khan[a], Asad Syed[b], Abu Ayoobul Ansary[c], Fuad Ameen[b], Omar H.M. Shair[b], Mohd Sajid Khan[a,*]

[a] Nanomedicine & Nanobiotechnology Lab, Department of Biosciences, Integral University, Lucknow, 226026, India
[b] Department of Botany and Microbiology, College of Science, King Saud University, Riyadh, 11451, Saudi Arabia
[c] Biochemical Sciences Division, CSIR-National Chemical Laboratory, Pune, 411008, India

ARTICLE INFO

Article history:
Received 5 February 2017
Received in revised form 21 August 2017
Accepted 6 September 2017
Available online 7 September 2017

Keywords:
B-AuNPs
B-AuNPs conjugated CIS and DOX
Cisplatin
Doxorubicin
Cytotoxicity
Osteosarcoma

ABSTRACT

Osteosarcoma or osteogenic sarcoma is the most common and prevalent cancerous tumor of bone and occurs especially in children and teens. Recent treatment strategy includes a combination of both chemotherapy and surgeries. Although, the use of single drug-based chemotherapy treatment remains unsatisfactory. Therefore, combinatorial therapy has emerged as a potential strategy for treatment with limited side- effects. Here, we evaluated the combinatorial anticancerous effect of cisplatin (CIS) and doxorubicin (DOX) bioconjugated bromelain encapsulated gold nanoparticles (B-AuNPs conjugated CIS and DOX) in the treatment of osteosarcoma. The synthesized B-AuNPs conjugated CIS and DOX were characterized by various characterization techniques like UV–vis spectroscopy, TEM, DLS and zeta potential to ensure the synthesis, size, shape, size distribution and stability. Drug loading efficiency bioconjugation of CIS and DOX was ensured by UV–vis spectroscopy. Bioconjugation of CIS and DOX was further confirmed using UV–vis spectroscopy, TEM, DLS, Zeta potential and FT-IR analysis. The combinatorial effect of CIS and DOX in B-AuNPs conjugated CIS and DOX showed highly improved potency against MG-63 and Saos-2 cells at a very low concentration where primary osteoblasts didn't show any cytotoxic effect. The apoptotic effect of B-AuNPs conjugated CIS and DOX on osteosarcoma and primary osteoblasts cells were analyzed by increased permeability of the cell membrane, condensed chromatin and deep blue fluorescent condensed nucleus. The results clearly showed that B-AuNPs conjugated CIS and DOX significantly improved the potency of both the chemotherapeutic drugs by delivering them specifically into the nucleus of cancer cells through caveolae-dependent endocytosis. Thus, the greater inhibitory effect of combinatorial drugs (B-AuNPs conjugated CIS and DOX) over single drug based chemotherapy would be of great advantage during osteosarcoma treatment.

1. Introduction

Osteosarcoma/osteogenic sarcoma is the most prevalent malignant and aggressive tumor of bone that occurs primarily in the long bones, particularly the proximal tibia and distal femur and especially occurs in adolescents and children aged between 10 to 24 years [1,2]. Although various conventional therapies such as radiotherapy, chemotherapy and surgical resection have evolved and made significant progress in osteosarcoma treatment (5-year survival rate to 65%), they are always associated with severe side effects. The prognosis of patients with osteosarcoma is still poor and up to 20% patients are diagnosed only at metastatic stage which is the biggest cause of concern [3]. Besides significant progress in osteosarcoma treatment, still, there is no substantial improvement occurring in osteosarcoma treatment and remains elusive [4]. The mainstay osteosarcoma treatment is the single drug based chemotherapy which leads to drug resistance [5].

Therefore, combinatorial therapy has been considered as a promising treatment method to minimize the side-effects and improve the therapeutic efficiency of drugs [6]. In combination therapy, anticancerous drugs believed to act synergistically towards suppression of cancer cells. The adaptations of cancer cells can be delayed by administration of chemotherapeutic drugs with different molecular pathways and further reduce the mutations in cancer cells. Anticancerous drugs with similar molecular pathways could act synergistically towards higher target selectivity and bet-

* Corresponding author.
E-mail address: research.sajid@gmail.com (M.S. Khan).

http://dx.doi.org/10.1016/j.colsurfb.2017.09.017
0927-7765/

ter therapeutic efficiency [7]. In this study, a unique combination of CIS and DOX was selected to improve their effect in the treatment of osteosarcoma. CIS is one the most potent anticancer drug against osteosarcoma and lung cancer. Its acts on DNA and eventually triggers several signal transduction pathways which include p53, p73, MAPK and ATR and finally lead to activation of apoptosis [8]. Nephropathy and drug resistance are two major side effects of CIS. DOX (an anthracycline), a very potent anticancer drug, works by generating free radicals which damage DNA, protein and cell membrane [9]. It also interrupts topoisomerase II- mediated DNA repair and intercalates into DNA [10]. Its side effects include cardiomyopathy, secondary malignancies extravasations and tissue necrosis, etc.

The administration of anticancerous drugs in combination did not result in improved therapeutic efficacy, despite the significance of combination therapy [11]. The diversity in biodistribution, pharmacokinetics and membrane transport mechanism of two anticancer drugs would result in extreme difficulty in dosing and poor accumulation in cancerous cells [12]. Therefore, it is necessary to entrap/conjugate multiple anticancerous drugs to a single nanocarrier so that it can help in the release of drug molecules in a predetermined manner. In this regard, nanocarrier used should have high loading capacity for both anticancerous drug and remain stable for a longer period in the bloodstream to avail enhanced retention (EPR) effect and permeability [13]. There have been various nanoparticles- based delivery strategies have been developed such as PEGylated PLGA NP-encapsulated paclitaxel and etoposide used against osteosarcoma [14], camptothecin-containing nanoparticle drug conjugated with bevacizumab against renal cell carcinoma [15], Doxorubicin conjugated bisphosphonate nanoparticles against osteosarcoma [16], methoxy-poly (ethylene glycol) aldehyde conjugated with doxorubicin and curcumin against Hep G-2 cancer cells [17] and doxorubicin-carbonane conjugated polymeric nanoparticles used for cancer therapy [18]. Nanoparticles with size (<200 nm) can abscond from reticuloendothelial system (RES) and circulate in the blood for prolonged time periods and through enhanced permeation and retention effect (EPR) nanoparticles can accumulate at the tumor site [19] as compared to conventional drugs. Among various nanoparticles, gold nanoparticles were selected because of their perceived non toxic nature, biocompatibility, tunable surface chemistry due to which additional functional groups can be conjugated [20]. Gold nanoparticles have the property of a large surface to volume ratio, which gives an ample number of anticancerous drug molecules being delivered to cancer cells.

Entry of nanoparticles into the cell is a very dynamic process and almost all endocytic pathways are energy dependent processes [21]. It depends upon physical and interfacial characteristics of NPs such as surface charge, size, shape and hydrophobicity. It also depends on cell type and properties of plasma membranes [22] such as receptor density, receptor type, the recycling rate of receptors and membrane fluidity [23]. Interactions of NPs and cell membranes with the biological environment are also crucial for the process [24]. A number of pathways may be used simultaneously for the uptake of nanoparticles, although with varying efficiency. Nanoparticles which are recognized by opsonins, such as blood serum proteins, complement component (C3, C4, and C5) and immunoglobulin (IgG and IgM), take phagocytosis route of cell entry after binding with cell surface receptors. Eventually, the cargo fuse with lysosomes and [25] destroyed by acidification and enzymolysis in the lysosomes. Therefore, to produce desired effects, nanomedicines must by pass this route to avoid degradation. Cell uptake studies revealed that the surface charge has a remarkable role in the uptake of nanoparticles.

Since, targeted drug delivery to cancerous cells is a highly appealing application of nanotechnology. Hence, tumor targeting by using nanosystems has come up with a variety of advantages, including reduced side effects, improved cancer bearing survival rate enhanced tumor targeting and elevated drug uptake [26]. Certain nanomedicines (or nanosystems) with FDA approval have been emerged and shown better clinical performance than traditional drugs [27]. Further, it has been proved that stable gold bioconjugates work exceptionally better than the pure drugs at a much lower concentration with substantially reduced side effects [28]. Since, CIS and DOX are highly effective, but with severe side effects and follow the almost same mode of action and form DNA adducts. Hence, a noble delivery system (B-AuNPs conjugated CIS and DOX) has been developed to deliver these drugs specifically into the nucleus of the cancer cells.

The present study investigates the enhanced, and the synergistic effect of the uniquely combined CIS and DOX conjugated bromelain (cysteine protease) encapsulated gold nanoparticles (B-AuNPs conjugated CIS and DOX). In this regard, we hypothesized those two anticancerous drugs (CIS and DOX), when administered together would significantly increase therapeutic efficiency in cancer treatment. The characterization of B-AuNPs conjugated CIS and DOX and bioconjugation of CIS and DOX was confirmed by UV–vis spectroscopy, DLS, Zeta potential, TEM, and FTIR analyses. The drug loading efficiency was calculated by UV–vis spectroscopy method. The cytotoxic effect of B-AuNPs, B-AuNPs conjugated CIS and DOX, and individual drugs evaluated on osteosarcoma cells (MG-63and Saos-2) and primary osteoblasts cells using MTT assay. Apoptotic effect of B-AuNPs conjugated CIS and DOX further confirmed by DAPI staining.

2. Materials and methods

2.1. Materials

2.1.1. Chemicals and reagents

Tetrachloroauric [III] acid ($HAuCl_4$), cisplatin, doxorubicin and bromelain were bought from Sigma-Aldrich. Unless stated otherwise, all chemicals and solvents were of analytical grade and were utilized as received.

2.2. In vitro *synthesis of B-AuNPs by using bromelain as reducing and capping agent*

In vitro synthesis of B-AuNPs was done by taking reaction mixtures of 3 ml, each containing 1 mM [$HAuCl_4$] [prepared in Phosphate buffer (50 mM)] and 1 mg/ml freshly prepared bromelain. The reaction mixture was incubated at 40 °C for 48 h. For control, a separate reaction completed in the absence of bromelain. The reaction mixture was removed at regular intervals of time and analysis was done by UV–vis spectroscopy to confirm the synthesis of nanoparticles. After the reaction completion, 50% v/v of ethanol treatment was used to remove unbound bromelain, and further by centrifugation (30,000*g*, 30 min) nanoparticles were collected, reaction mixture washed twice using Milli-Q water and used for further characterization.

2.3. *Bioconjugation of B-AuNPs with a combination of cisplatin and doxorubicin*

In vitro, synthesized gold nanoparticles were bioconjugated to the mixture of anticancerous drugs cisplatin and doxorubicin. The activator 1-Ethyl-3-(3-dimethyl) carbodiimide (EDC) used to bind the free amino group(s) of all the anticancerous drugs with the carboxylate group(s) present on bromelain [29]. The 5 ml reaction mixture containing 50 mM HEPES buffer, 250 μg drugs (125 μg CIS + 125 μg DOX), and 250 μg of B-AuNPs was used for coupling

whereas 5 mM EDC was added in aliquots within 3 h at 30 °C in the reaction mixture.

2.4. Determination of loading efficiency (LE) of CIS + DOX on B-AuNPs by UV–vis spectrophotometry

The total loading percentage of cisplatin and doxorubicin was estimated by examining the change in the intensity of the wavelength, before and after bioconjugation, at 300 nm (λ_{300} nm) for cisplatin [30] and at 481 nm (λ_{481} nm) for doxorubicin [31]. These absorbance would be finally added together to know the total loading percentage of drugs on B-AuNPs.

The loading percentage of CIS and DOX were estimated by putting the values of A and B in Eq. (1). The loading efficiency of each drug calculated one by one using Eq. (1). The absorbance of CIS at 300 nm and DOX at 481 nm determined and finally added together:

$$\%\text{LoadingofanticancerousdrugsonB-AuNPs} = [(A - B)] * 100/A \quad (1)$$

Where A is the absorbance of total drug added to B-AuNPs, B is the absorbance of drug after conjugation in supernatant of B-AuNPs conjugated CIS and DOX and both A and B were measured at the respective O.D. of each drug [32].

The standard curve of CIS and DOX at 300 nm and 481 nm was established respectively, and unbound drug was calculated from the standard curve. The amount of bioconjugated drugs was calculated by subtracting unbound drug from the total amount of drug added. The exact amount of bioconjugated drugs was calculated using Eq. (2).

$$\%\,\text{Bioconjugation} = \frac{\text{Amount of drug bioconjugation}}{\text{Total drug added}} \times 100 \quad (2)$$

2.5. Characterization of in vitro synthesized B-AuNPs conjugated CIS and DOX by various techniques

UV–vis spectrophotometry measurements were performed on a Shimadzu dual-beam spectrophotometer (model UV-1601 PC), operated at a resolution of 1 nm. Transmission Electron Microscopy (TEM) was done on Tecnai^{TM} G^2 Spirit BioTWIN FEI Company operated at an accelerating voltage of 80 kV. The sample was prepared by drying a drop of B-AuNPs conjugated CIS and DOX solution on carbon coated TEM copper grids followed by measurements on TEM. The mean particle size of conjugated B-AuNPs conjugated CIS and DOX was measured with a dynamic light scattering (DLS) particle size analyzer (Zeta Sizer Nano-ZS, Model ZEN3600, Malvern Instrument Ltd, Malvern, UK). The sample was taken in a DTS0112-low volume disposable sizing cuvette of 1.5 ml. The sample powder was diluted to a concentration of 0.5% (w/v) in deionised water. The particles were sonicated by using Sonic & Material Inc., New Town, CT, USA at 30 W for 1 min (20 s on and 5 s off). Mean particle size was the average of triplicate measurements for a single sample. The surface charge of B-AuNPs conjugated CIS and DOX was measured using a Zeta Sizer Nano-ZS, Model ZEN3600 (Malvern Instrument Ltd, Malvern, UK). The confirmation of binding and secondary structure of bromelain at the surface of GNPs and subsequently, bioconjugated B-AuNPs conjugated CIS and DOX was done by Fourier transform infrared spectroscopy (FTIR). A bromelain-Au film on a Si (111) substrate was prepared by placing a drop of B-AuNPs conjugated CIS and DOX solutions on a Si (111) substrate and evaporation of water were performed by gentle heating and FTIR spectra of the film were recorded on a Shimadzu FTIR-8201 PC instrument operated in the diffuse reflectance mode at a resolution of 4 cm^{-1}. To obtain good signal-to-noise ratios, 256 scans of the bioconjugate film were taken in the range 400–4000 cm^{-1}.

2.6. Cell culture

The human osteogenic sarcoma cell lines MG-63, and Saos-2 were purchased from National Centre for Cell Science (NCCS), Pune, India. The primary osteoblasts were isolated from calvaria of neonatal rat by enzymatic digestion. Primary osteoblast cells, MG-63, and Saos-2 were grown as a monolayer in MEM, EMEM, and McCoy's media, respectively, supplemented with 10% FBS (fetal bovine serum) and 1% antibiotics (10,000 units of penicillin, 25 μg amphotericin B, and 10 mg streptomycin) in an incubator with a humidified atmosphere containing 5% CO_2 at temperature of 37 °C. All the cell stocks were maintained in 25 cm^2 tissue culture flask.

2.7. Cell viability assay

Primary osteoblast, MG-63, and Saos-2 cells were plated in a 96 well plate at a density of 1×10^4 cells per well and kept for incubation of 24 h in a humidified 5% CO_2 incubator at 37° C. After the incubation, the cells were treated with B-AuNPs conjugated CIS and DOX, pure doxorubicin, pure cisplatin served as a positive control at (1, 0.5, 0.25, 0.125, 0.0625 μg/ml) and with a concentration in triplicates, and again incubated for 48 h. After 48 h, the media was removed and 50 μl of 3-(4,5-dimethylthiazol-2-yl)-2,5-diphenyltetrazolium bromide (MTT) stain (5 mg/ml in PBS), was added to all wells. The plate was incubated for 4 h in 5% CO_2 incubator. The formazan crystals formed were dissolved in 150 μl DMSO (Dimethyl sulfoxide). The quantification of reduced MTT was performed by measuring the optical densities at a wavelength of 570 nm with a reference filter of 655 nm using an ELISA reader [Microplate Reader (BIORAD-680)]. The Percentage inhibition of the cells was calculated using the formula

$$X = 100 - (A_{test} - A_{blank})/(A_{control} - A_{blank}) \times 100;$$

Where. X- percentage inhibition, A_{test} − absorbance of the test sample, A_{blank} − absorbance of blank and $A_{control}$ − absorbance of the control sample. The IC_{50} value was calculated by fitting the data using ORIGIN 6.1

2.8. Analysis of cytomorphological changes in osteosarcoma and primary osteoblast cells

Primary osteoblast, MG-63, and Saos-2 cells were pre-treated with different concentration of B-AuNPs, B-AuNPs conjugated CIS and DOX and also with pure cisplatin, doxorubicin incubated for 48 h at 37 °C in 5% CO_2 atmosphere. After the incubation period, the overall changes in the cells morphology were observed under an inverted phase contrast microscope (Nikon ECLIPSE Ti-S, Nikon Corporation, Tokyo Japan).

2.9. Assessment of changes in nuclear morphology in osteosarcoma and primary osteoblast cells

The apoptotic effect of biogenic B-AuNPs conjugated CIS and DOX on primary osteoblast, MG-63, and Saos-2 cells was assessed by using fluorescent nuclear stain DAPI. The osteosarcoma and primary osteoblast cells were seeded in 96 well plate and treated as mentioned above in cell viability assay. Further, the cells were washed with phosphate buffer saline (PBS) and fixed with 4% paraformaldehyde for 10 min. Subsequently, the permeabilizing buffer (3% paraformaldehyde and 0.5% Triton X-100) was used for permeabiliztion of fixed cells and stained with DAPI. After DAPI staining, the cell images were obtained with a fluorescence microscope (Nikon ECLIPSE Ti-S, Japan). The cells with condensed and fragmented nuclei were considered as apoptotic cells.

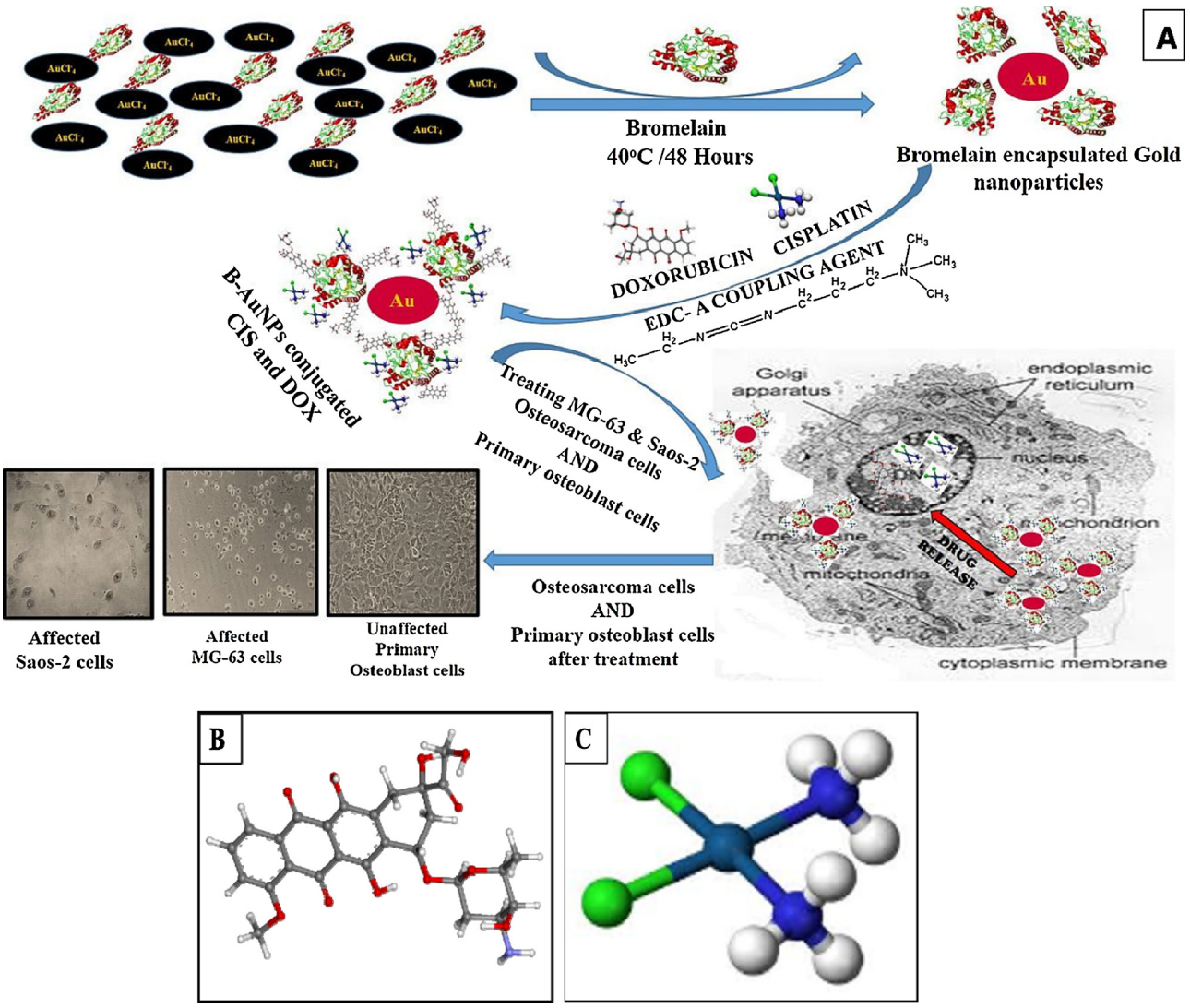

Fig 1. Schematic diagram (A) Bromelain assisted synthesis of gold nanoparticles conjugated with anticancerous drug cisplatin and doxorubicin to combat Saos-2 and MG-63 bone cancer cells and no change in primary osteoblasts. Internalization of B-AuNPs conjugated CIS and DOX may be through passive as well as active process (B) 3D structure of doxorubicin and (C) 3D structure of cisplatin.

3. Results and discussion

In this study, bromelain encapsulated biogenic gold nanoparticles have been bio conjugated with cisplatin and doxorubicin to combat against bone cancer. The schematic representation of whole study has been presented in Fig. 1.

3.1. Enzymatic synthesis of B-AuNPs and their bioconjugation with CIS and DOX

Bromelain (a cysteine protease) was used to reduce auric chloride into gold nanoparticles. This is a bottom up approach where bromelain works as a reducing as well as a capping agent. Desired sizes of monodispersed nanoparticles can be obtained by regulating the concentration of bromelain, temperature of reaction and incubation time. The spectral studies of B-AuNPs showed an intense peak at 527 nm (Fig. 2A). The SPR absorption band of B-AuNPs conjugated CIS and DOX and B-AuNPs were plotted in Fig. 2A. B-AuNPs conjugated CIS and DOX have shown a decrease in intensity of the peak with a noticeable red shift from 527 nm to 531 nm (Fig. 2A) in comparison to B-AuNPs. The red or blue shift in SPR confirms a change in the surface chemistry of B-AuNPs due to bioconjugation of CIS and DOX on their surface.

3.2. Characterization of B-AuNPs conjugated CIS and DOX

3.2.1. TEM, DLS and zeta potential

TEM micrographs (Fig. 2B) confirmed the increase in size of B-AuNPs conjugated CIS and DOX in comparison to B-AuNPs (~9.2 nm) and were found to be ~9.9 nm. This also confirmed that B-AuNPs conjugated CIS and DOX were spherical in shape, monodispersed and uniformly distributed. TEM calculates the size of nanoparticles by directly transmitted electrons which give the information about only inorganic core and doesn't include hydration layer. Further, DLS was conducted to estimate the increase in hydrodynamic radius of B-AuNPs conjugated CIS and DOX in comparison to B-AuNPs (54.76 nm) and was found to be 65.23 nm (Fig. 2C). When nanoparticles are moved through a liquid, their surfaces will be shielded by a thin electric dipole layer of the solvent. Therefore, when the sizes of nanoparticles are measured under DLS, it estimates hydrodynamic diameter of particles and provides information of the inorganic core along with coating material and the solvent layer attached to the particle. As a result, the size study

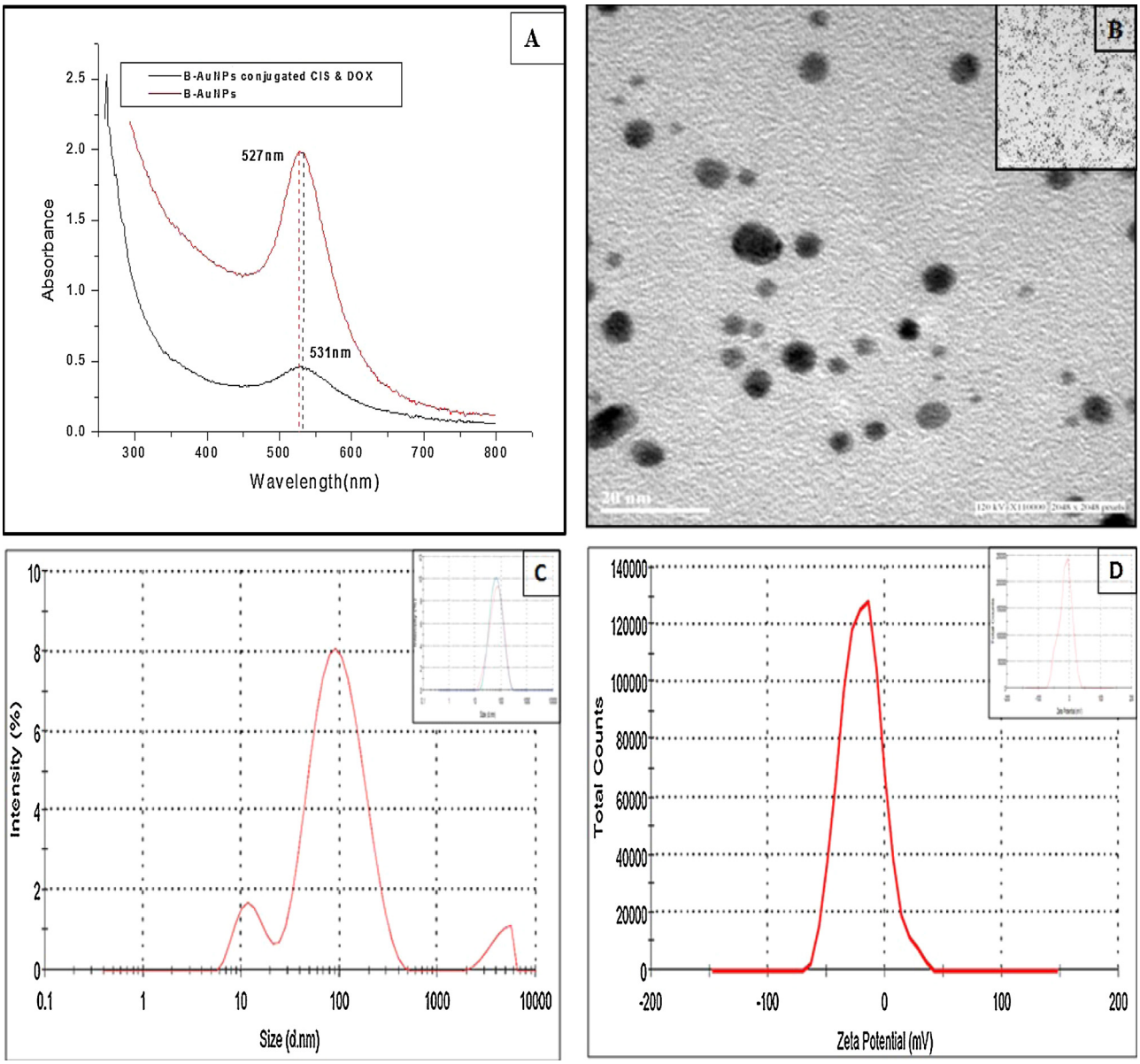

Fig. 2. Characterization of B-AuNPs conjugated CIS and DOX under (A) UV–vis spectra (B) DLS (C) Zeta potential (D) TEM.

given by DLS technique and TEM is not similar ever [33]. Zeta potential can easily provide the information about the concentration, distribution, exposure or shielding of charged moieties, ionization, adsorption [34] of the nanoparticles. The change in zeta potential of B-AuNPs conjugated CIS and DOX was also observed and it was found to be −13.3 mV (Fig. 2D) whereas the zeta potential for B-AuNPs was measured to be −19.5 mV. The negative charge on nanoparticles may be due to the functional groups present in the amino acids of bromelain, which confirms the high stability of B-AuNPs and B-AuNPs conjugated CIS and DOX. All the changes further confirm the bioconjugation of CIX and DOX with B-AuNPs.

3.2.2. FTIR spectroscopy

FTIR spectroscopy was employed to evaluate the presence of CIS and DOX on the surface of the B-AuNPs. The spectrum obtained from B-AuNPs conjugated CIS and DOX was compared to the spectra of B-AuNPs, pure cisplatin and doxorubicin. The broadband contour which appears in the range 3600–3000 cm^{-1} is due to the −NH stretch of a peptide bond. The peaks at 1760 and 1570 cm^{-1} represent —C═O anhydride stretching vibration. The spectra also showed a peak shift of carboxylic stretch (C═O) from 1641 to 1622 cm^{-1} suggesting the intermolecular interactions between drugs and B-AuNPs (Fig. 3A). The characteristic peaks of CIS from 1600 to 1500 cm^{-1} (asymmetric amine bending) and 1300–1200 cm^{-1} (symmetric amine bending) were also observed in the spectra [35]. The emergence of new peaks at 1285 cm^{-1} (C—O—C stretching), 1407 cm^{-1} (C—C stretching), 1442 cm^{-1} (coupling of C—N and N—H), 996 cm^{-1} (C—O stretching) can be attributed to conjugation of DOX [36] and CIS to B-AuNPs.

3.2.3. Drug loading efficiency

The percentage loading of CIS on B-AuNPs conjugated CIS and DOX has been calculated by using Eq. (1) and found to be ~47.5% indicating efficient binding of the drug to B-AuNPs. The values of A and B were obtained as 0.040 and 0.021 respectively and substituted in Eq. (1)

The percentage loading of DOX on B-AuNPs conjugated CIS and DOX has also been calculated by using Eq. (1) and found to be ~34.4% indicating efficient binding of the drug to B-AuNPs. The val-

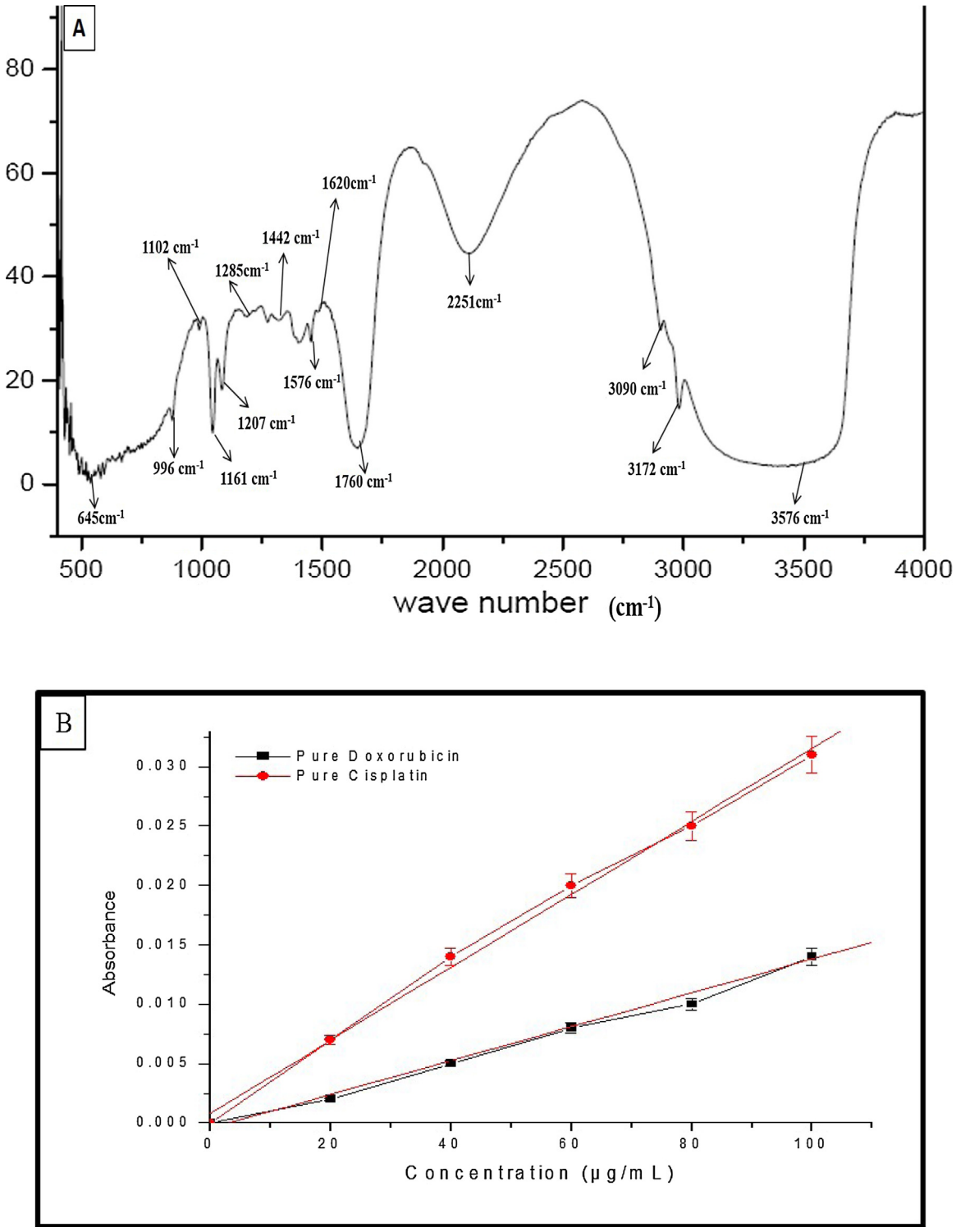

Fig. 3. (A) FTIR spectra of B-AuNPs conjugated CIS and DOX (B) UV–vis spectra of pure cisplatin and doxorubicin.

ues of A and B were obtained as 0.090 and 0.050 respectively and substituted into Eq. (1)

The standard curve of pure CIS and DOX was established at 300 nm and 481 nm respectively, and unbound drug was calculated from the standard curve. The amount of bioconjugated drugs was calculated by subtracting unbound drug from the total amount of drugs added. The exact amount of total bioconjugated drugs was calculated by adding the percentage loading of CIS and DOX by using Eq. (2) and was found to be 81.9% (Fig. 3B).

*3.2.4. Anticancer studies of B-AuNPs and B-AuNPs conjugated CIS and DOX (*in vitro*)*

3.2.4.1. Cell viability. The *in-vitro* cytotoxic effect of B-AuNPs, B-AuNPs conjugated CIS and DOX, pure DOX and pure CIS were evaluated on MG-63 and Saos-2 osteosarcoma cell lines at different concentrations (1, 0.5, 0.25, 0.125, 0.0625 µg/ml) by using MTT assay (Fig. 4) whereas primary osteoblasts cells were taken as controls [37]. The cytotoxic effect of B-AuNPs conjugated CIS and DOX on cell lines was dose dependent. In MG-63 cells, with increase in

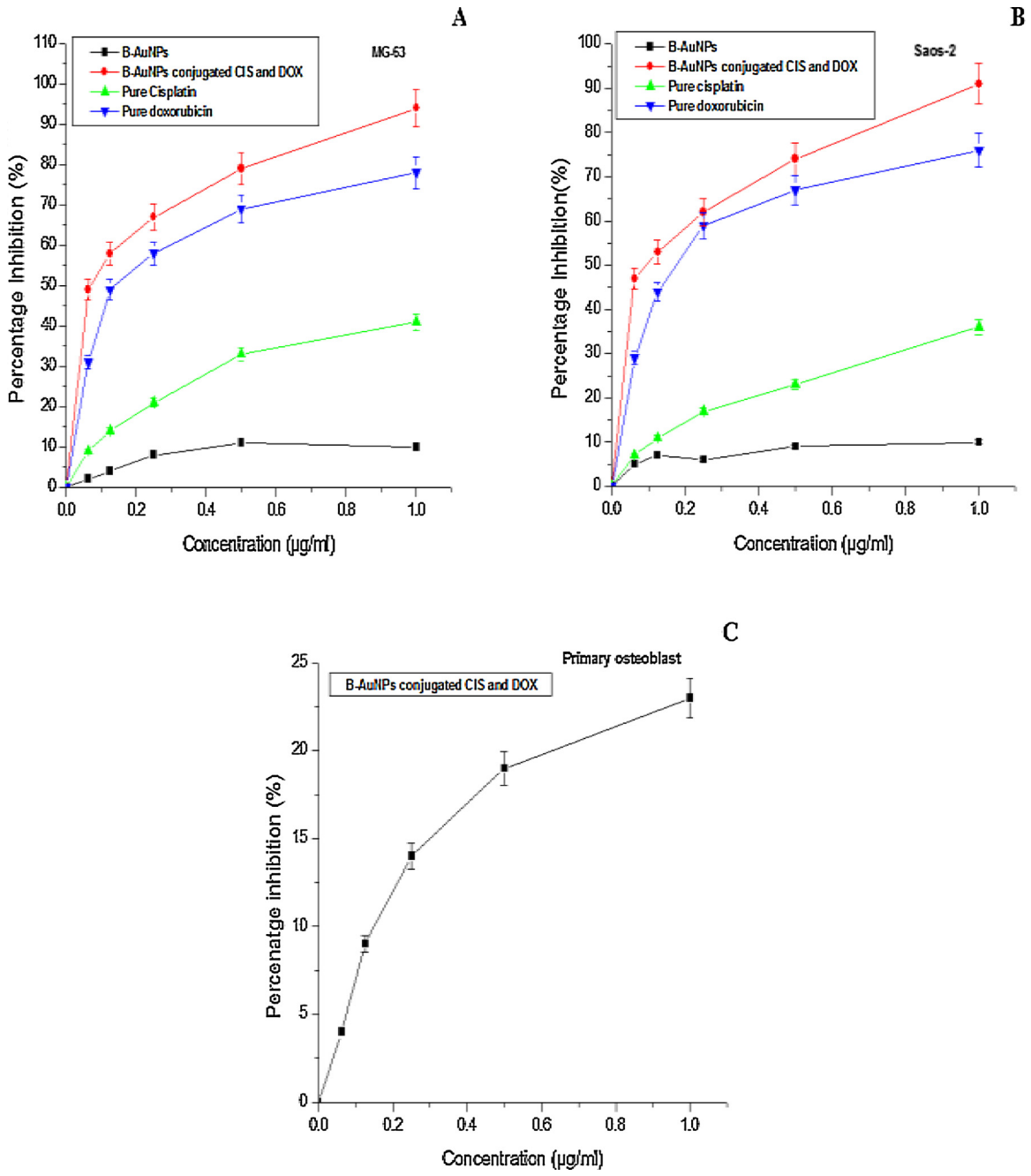

Fig. 4. The cytotoxicity (dose dependent) study of B-AuNPs, B-AuNPs conjugated CIS and DOX on (A) MG-63 (B) Saos-2 and, (C) primary osteoblasts cells. B-AuNPs conjugated CIS and DOX inhibited cell growth significantly of Saos-2 and MG-63 with IC_{50} values 0.09 μg/ml, 0.07 μg/ml respectively and IC_{50} values of pure doxorubicin on Saos-2 and MG-63 were found to be 0.177 μg/ml and 0.144 μg/ml respectively but did not affect primary osteoblast cells significantly, while B-AuNPs and pure cisplatin had also shown no cytotoxic activity on Saos-2 and MG-63. All the data were expressed in mean ± SD of three experiments.

concentration of B-AuNPs conjugated CIS and DOX from 0.0625, 0.125, 0.25, 0.5 to 1 μg/ml, the anticancerous effect also increases from 49%, 58%, 67%, 79%, to 94%, respectively. Similarly, in Saos-2 cells with increase in concentration from 0.0625, 0.125, 0.25, 0.5 to 1 μg/ml, the anticancerous effect also increases from 47%, 53%, 62%, 74%, to 91%, respectively. The analyzed results revealed substantially good effects with IC_{50} values of B-AuNPs conjugated CIS and DOX over pure DOX and pure CIS, which were found to be 0.071 μg/ml and 0.09 μg/ml on MG-63 and Saos-2 cells, respectively (Fig. 4A, B). B-AuNPs conjugated CIS and DOX showed no significant toxicity on primary osteoblasts cells (Fig. 4C). The IC_{50} values of pure doxorubicin on MG-63 and Saos-2 were found to be 0.144 μg/ml and 0.177 μg/ml respectively (Fig. 4A, B). B-AuNPs (up to 10%) and pure CIS (up to 41%) treated osteosarcoma cells (MG-63 and Saos-2) showed no significant toxicity at the given concentration.

3.2.5. Cytomorphological changes in B-AuNPs conjugated CIS and DOX and B-AuNPs treated MG-63, Saos-2, and primary osteoblasts cells

The morphological changes were analyzed using Image Tools software. The change in cell's shape was determined with the degree of roundedness of the cell which is one of the important stress indicators (Fig. 5). Osteosarcoma (Saos-2 and MG-63) cells were treated with B-AuNPs conjugated CIS and DOX, B-AuNPs, pure DOX and pure CIS for a period of 48 h and their cytomorphological

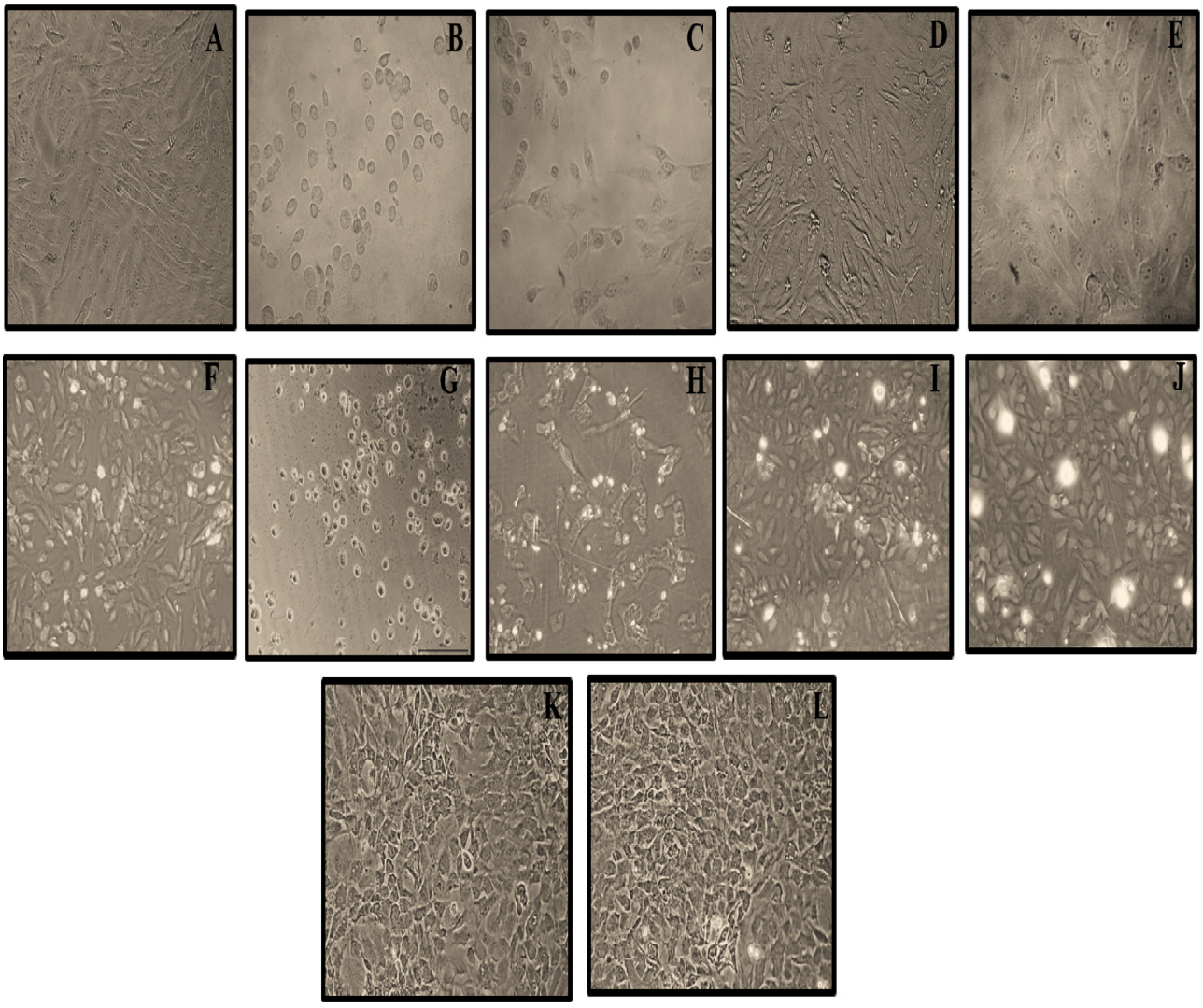

Fig. 5. Images showing MG-63 cells (A) Control (B) treated with B-AuNPs conjugated CIS and DOX (C) treated with pure doxorubicin, (D) treated with B-AuNPs (E) treated with pure cisplatin also, Saos-2 cells (F) Control (G) treated with B-AuNPs conjugated CIS and DOX (H) treated with pure doxorubicin (H), treated with B-AuNPs (I) treated with pure cisplatin and also, Primary osteoblast cells (K) Control, (L) treated with B-AuNPs conjugated CIS and DOX, under phase contrast microscope after 48 h of treatment.

observations (Fig. 5) revealed that after 48 h of treatment, most of the cells treated with B-AuNPs conjugated CIS and DOX (Fig. 5B, G) and pure DOX (Fig. 5C, H) changed their normal shape, many cells detached from substratum and came into suspended culture media, while others have shown clear blebbing characteristics. The number of live control cells was much higher than the treated cells (Fig. 5A, F, K). B-AuNPs and pure CIS showed no significant change in cell shape on MG-63 and Saos-2 cells (Fig. 5D, I). Further, B-AuNPs conjugated CIS and DOX also showed no significant effect on primary osteoblasts morphology (Fig. 5L).

3.2.6. Assessment of changes in nuclear morphology in osteosarcoma and primary osteoblast cells

The mechanism of cellular uptake and internalization of B-AuNPs conjugated CIS and DOX was further analyzed by using a fluorescent stain 4′, 6-diamidino-2-phenylindole (DAPI). The route of cellular uptake of B-AuNPs conjugated CIS and DOX could be through endocytosis followed by the drug release to B-AuNPs from endosome/lysosome into the cancerous cells, where the reaction between DOX/CIS and DNA takes place [38]. In this regard, osteosarcoma cells (MG-63 and Saos-2) and primary osteoblasts cells were incubated with B-AuNPs conjugated CIS and DOX for 24 h at 37° C and further stained with DAPI. The osteosarcoma cells (MG-63 and Saos-2) and primary osteoblasts cells treated with B-AuNPs conjugated CIS and DOX caused an apoptotic effect in the cells and increased the permeability; that resulted in condensed chromatin and deep blue fluorescent condensed nucleus of MG-63 and Saos-2 cells (Fig. 6B & D) as compared to their controls (Fig. 6A & C). The most significant and selective sign of cytotoxic effect caused by stress is the nucleus condensation [39]. B-AuNPs conjugated CIS and DOX treated primary osteoblasts cells (Fig. 6F) showed no difference as compared to control (Fig. 6E).

3.3. Proposed mechanism

Though highly effective against cancer, cisplatin (due to failure of Na^+, K^+-ATPase) also causes nephrotoxicity and develop resistance against tumor during therapy. Cisplatin inhibits DNA replication by forming a bifunctional adduct (covalent bonds between DNA purine base (N_7 position) and platinum atom of CIS-forms inter and intra strand cross links) which, eventually, initiates cell apoptosis [40]. If CIS is internalized intact into the cell, it will be most effective and hence, requires very low concentration for the substantial effect. Similarly, DOX, another highly effective approved agent against wide range of cancers, including breast, prostate, lymphoma, sarcoma and leukaemia [41], intercalates with

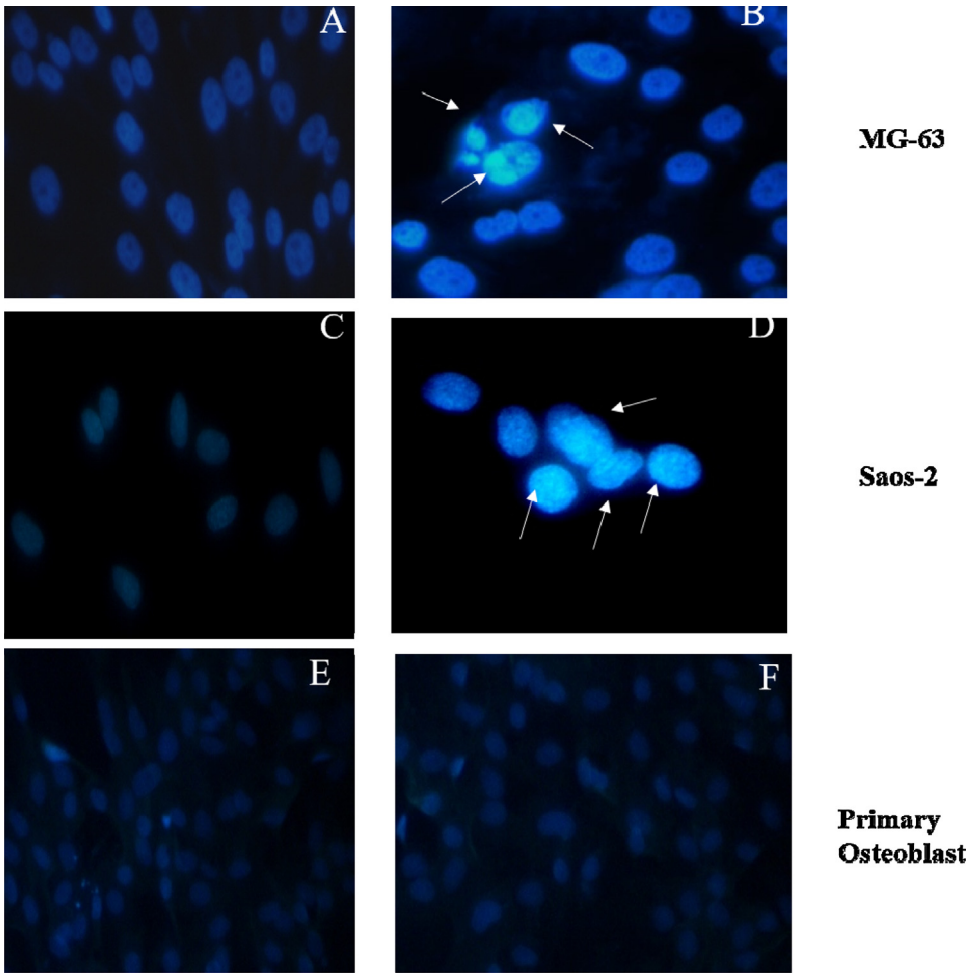

Fig. 6. DAPI Staining on Saos-2, MG-63 and Primary osteoblasts cells to check apoptosis by B-AuNPs conjugated CIS and DOX (A) Control of MG-63 cells (B) MG-63 cells treated with B-AuNPs conjugated CIS and DOX, (C) Control of Saos-2 cells (D) Saos-2 cells treated with B-AuNPs conjugated CIS and DOX (E) Control of primary osteoblasts cells (F) Primary osteoblasts cells treated with B-AuNPs conjugated CIS and DOX. Scale bar −100 μm, Magnification- 20X; Apoptotic cells (white arrow).

DNA; inhibits topoisomerase II and eventually forms adducts which lead to the cell apoptosis [42]. But doxorubicin is non- specific in action due to lack of cancer cell recognition. It also perishes normal cells with the same effect and causes severe side effects.

In this study, a noble bromelain (cysteine protease) encapsulated gold nanoparticles bioconjugated with CIS and DOX (B-AuNPs conjugated CIS and DOX) inhibited the growth of bone cancer cell lines (Saos-2 and MG-63) without affecting the growth of primary osteoblasts cells even when treated with nanoparticles at high concentrations. The osteosarcoma/osteogenic sarcomadevelops from osteoblasts cells is characterized by an array of markers which are differentially expressed. The two osteogenic sarcoma cell lines (MG-63 and Saos-2) have most of the markers common, except few markers such as ALP, Collagen II, CollagenVI, and Collagen IX, etc. [43]. The osteogenic sarcoma cells (MG-63 and Saos-2) are dissimilar from primary osteoblasts cells only in marker i.e. MMP-9, while all other markers are either same in one or both the osteosarcoma cell lines [44,27]. The role of interactions of B-AuNPs conjugated CIS and DOX nanoparticles with the cell surface receptors is very critical not only in the internalization of nanoparticles but also involves in selectively inhibition in the progression of cells. It is highly possible that B-AuNPs conjugated CIS and DOX nanoparticles interact with one of the cell surface receptors, since there are various receptors in osteosarcoma which are highly overexpressed like, Wnt coreceptors LRP5, hepatocyte growth factor (HGF)/MET, insulin-like growth factor (IGF), platelet-derived growth factor (PDGF) and/or its receptor platelet-derived growth factor receptor (PDGFR), bone morphogenetic protein (BMPs) and/or its receptor bone morphogenetic protein receptor (BMPRs), and fibroblast growth factor (FGF)/fibroblast growth gactor receptor (FGFRs) [43]. It is worth noting that over-expression of PDGF/PDGFR, which is needed to regulate normal proliferartion of osteoblastic cells, favors proliferation of cells in osteosarcoma [43]. Further, in osteosarcoma formation the connective tissue growth factor (CTGF) is up-regulated in osteogenic sarcoma cells [45] to regulate the undifferentiated status and it may also be involved in deregulation of angiogenic pathways (predominantly, HIF1 α and VEGF) [46]. The overexpression of certain other cell surface receptors such as Wnt/β-catenin is correlated with metastases of osteosarcoma and osteoprogenitor proliferation [47]. The up-regulation of Wnt may also induce chemoresistance by the repression of a bone matrix syndecan-2, proteoglycan [48].

The gold nanoparticles were chosen as a vehicle for drug delivery system because they did not show any significant toxicity up to 10^{12} particles/ml concentration [49] and have the intrinsic properties to enhance the apoptosis of the cancer cells which are stable to programmed cell death. Being antiangiogenic in nature, the intravenous gold bioconjugates rapidly accumulates in the defected cells [50] and they are not detected in cells of the liver, spleen, and other healthy organs [51]. The use of bromelain as a reducing agent and also as a capping agent to synthesize gold nanoparticles of desired sizes is a great idea because it reduces auric chloride

strongly and form stable corona on the surface of as-synthesized gold nanoparticles. Bromelain (cysteine-protease) which belongs to the papain family and favourably cleaves leucyl, glycyl, and alanyl bonds where nucleophile of the catalytic site which usually acts as a base and is a part of histidine amino acid [52]. It acts systemically, affecting several molecular and cellular targets. Its high doses (10 g/kg) for prolonged periods of therapy can be used [53]. Being cysteine protease, it acts as an anticancer agent also. It is well known that it interacts with cell surface and regulates several signal pathways such as to increase neutrophil activity, down regulate NF-κB, Cox-2, PGE-2 [54] and TGF-β [55]; upregulates p53 and Bax [56]; the activity of cell survival regulators decreases such as Erk, Akt and debilitate the FOXO3A (Akt- dependent Pro apoptotic regulator) [57]. It also reduces expression of CD44 on the cell surface of tumor [58]. Entry of traditional drugs (being small in size) takes place mainly via active transport or passive diffusion while nanomedicines take endocytosis as a mode of entry into the cells [59].

Non specific internalization of nanoparticles (both positive and negative) takes place through macropinocytosis which is a vesicular transmonolayer transport and uses dynamin and microtubule network. It starts with external stimulus which activates the receptor tyrosine kinase present on cell membrane. In brief, it is a transient, clatherin and caveolin-independent, growth factor-induced and actin-driven endocytosis [60,61]. Positively charged nanoparticles are preferably internalized by Clathrin pathway and macropinocytosis but caveolae dependent endocytosis does not involve into this process. Cationic NPs has the ability to directly bind to a negatively charged plasma membrane of cells [62], either bind with anionic head group of phospholipids or gets attached to other negatively charged groups present on the cell membrane, for instance monosaccharide sialic acid. The interaction of cationic nanoparticles with the cell membrane, they can induce internalization by a clathrin mediated endocytosis. The B-AuNPs conjugated CIS and DOX are negatively charged nanosystems and microdomains formed in the caveolar vesicles usually made up of cationic lipids such as sphingomyelin (an amine group present on its polar domain), can interact and mediate the anionic nanoparticle's endocytosis [63]. Thus, the internalization of B-AuNPs conjugated CIS and DOX (anionic in nature) takes place through caveolae dependent endocytosis and macropinocytosis but involvement of clatherin pathway was ruled out due to anionic charge of B-AuNPs conjugated CIS and DOX.

However, in the caveolae-mediated endocytosis, the nanoparticles do not fuse with lysosomes after their entry into cells, which not only prevent the drugs from degradation but also give them a chance to arrive into other organelles. After engulfed in the cells, the vesicles containing B-AuNPs conjugated CIS and DOX fuse with caveosomes or multivesicular body (MTV). The caveosomes containing B-AuNPs conjugated CIS and DOX move along with microtubules to the ER [64] and through ER it penetrates into the cytosol, and eventually enter into nucleus via the nuclear pore complex [65]. Clathrin-caveolae independent endocytosis also involves into the internalization of the B-AuNPs conjugated CIS and DOX. It is Arf6-dependent, Cdc42-dependent and Rhoa dependent pathway [66] and it depends on cholesterol and needs specific lipid compositions.

Thus, this is an ideal strategy to deliver intact (or without degradation) anticancer drugs specifically into the nucleus which act on DNA or enzymes required for replication of DNA which is critical for improvement of therapeutic delivery [67]. Also, size and shape of B-AuNPs conjugated CIS and DOX are ideal for internalization [68]. Thus, this cargo will be proved noble and substantially potent against osteosarcoma.

4. Conclusion

In the given research, a noble bromelain (cysteine protease) encapsulated gold nanoparticles bioconjugated with CIS AND DOX (B-AuNPs conjugated CIS and DOX) nanomedicine has been developed which was found highly stable, biocompatible and potent against osteosarcoma. Being negative in charge, this cargo can be easily internalized through almost all types of cells preferably by following caveolae mediated endocytosis which can deliver bioconjugated drugs into the nucleus without degradation where they can act directly on the DNA and form DNA adduct. Though, both the drugs follow almost same kind of mechanism to inhibit the progression of osteosarcoma cells. Hence, they act synergistically and their potency got improved substantially very high. Thus, we propose B-AuNPs conjugated CIS and DOX as a potent nanomedicine against osteosarcoma.

Acknowledgements

The author SI thanks University Grant commission (UGC), New Delhi, for Maulana Azad National Fellowship and MZ thanks UPCST for the scholarship. The authors also acknowledge Integral University and Department of Biosciences for providing facilities and support for the research. The authors extend their appreciation to the Deanship of Scientific Research at King Saud University for funding this work through research group No (RG-1438-078).

References

[1] Z.F. Xin, C.C. Shen, L.J. Jao, S.G. Yan, H.B. Wu, Gambogic acid inhibits invasion of osteosarcoma via upregulation of TIMP-1, Int. J. Mol. Med. 31 (2013) 105–112.
[2] V.A. Siclari, L. Qin, Targeting the osteosarcoma cancer stem cell, J. Orthop. Surg. Res. 5 (2010) 78.
[3] Y. Cheng, L. Cai, P. Jiang, J. Wang, C. Gao, H. Feng, C. Wang, H. Pan, Y. Yang, SIRT1 inhibition by melatonin exerts antitumor activity in human osteosarcoma cells, Eur. J. Pharmacol. 715 (2013) 219–229.
[4] J.K. Anninga, H. Gelderblom, M. Fiocco, J.R. Kroep, A.H. Taminiau, P.C. Hogendoorn, et al., Chemotherapeutic adjuvant treatment for osteosarcoma: where do we stand, Eur. J. Cancer 47 (2011) 2431–2445.
[5] J. Woodcock, J.P. Griffin, R.E. Behrman, Development of novel combination therapies, N. Engl. J. Med. 364 (2011) 985–987.
[6] T.M. Sun, J.Z. Du, Y.D. Yao, C.Q. Mao, S. Dou, S.Y. Huang, et al., Simultaneous delivery of siRNA and paclitaxel via Two-in-One micelle plex promotes synergistic tumor suppression, ACS Nano 5 (2011) 1483–1494.
[7] D. Lang, Designer combination therapy for cancer, Nat. Biotechnol. 24 (2006) 163–164.
[8] D. Perez-Callejo, J. Gonzalez-Rincon, A. Sanchez, M. Provencio, M. Sanchez-Beato, Action and resistance of monoclonal CD 20 antibodies therapy in B-cell Non-Hodgkin Lymphomas, Cancer Treat. Rev. 41 (2015) 680–689.
[9] E. Feinstein, E. Canaani, L.M. Weiner, Dependence of nucleic acid degradation on in situ free-radical production by Adriamycin, Biochemistry 32 (1993) 13156–13161.
[10] K.M. Tewey, T.C. Rowe, L. Yang, B.D. Halligan, L.F. Liu, Adriamycin-induced DNA damage mediated by mammalian DNA topoisomerase II, Science 226 (1984) 466–468.
[11] C.M. Hu, S. Aryal, L. Zhang, Nanoparticle-assisted combination therapies for effective cancer treatment, Ther. Deliv. 1 (2010) 323–334.
[12] J. Lehar, A.S. Krueger, W. Avery, A.M. Heilbut, L.M. Johansen, E.R. Price, et al., Synergistic drug combinations tend to improve therapeutically relevant selectivity, Nat. Biotechnol. 27 (2009) 659–666.
[13] N. Kolishetti, S. Dhar, P.M. Valencia, L.Q. Lin, R. Karnik, S.J. Lippard, R. Langer, O.C. Farokhzad, Engineering of self-assembled nanoparticle platform for precisely controlled combination drug therapy, Proc. Natl. Acad. Sci. U. S. A. 107 (2010) 17939–17994.
[14] B. Wang, X.C. Yu, S.F. Xu, M. Xu, Paclitaxel and etoposide co-loaded polymeric nanoparticles for the effective combination therapy against human osteosarcoma, J. Nanobiotechnol. 13 (2015) 22.
[15] S.M. Keefe, J. Hoffman-Censits, R. Cohen, D. Heitjan, S. Eliasof, A. Nixon, B. Turnbull, E.G. Garmey, O. Gunnarsson, M. Waliki, J. Ciconte1, L. Jayaraman, A. Senderowicz, A.B. Tellez, M. Hennessy, A. Piscitelli, D. Vaughn, A. Smith, N.B. Haas, Efficacy of the nanoparticle?drug conjugate CRLX101 in combination with bevacizumab in metastatic renal cell carcinoma: results of an investigator-initiated phase I–IIa clinical trial, Ann. Oncol. 27 (2016) 1579–1585.
[16] S. Rudnick-Glick, E. Corem-Salkmon, I. Grinberg, E. Gluz, S. Margel, Doxorubicin conjugated bisphosphonate nanoparticles for the therapy of Osteosarcoma, JSM Nanotechnol. Nanomed. 2 (2014) 1022.

[17] Z. Yumin, Y. Cuihong, W. Weiwei, L. Jinjian, L. Qiang, H. Fan, C. Liping, G. Honglin, L. Chen, K. Deling, L. Qian, L. Jianfeng, Co-delivery of doxorubicin and curcumin by pH-sensitive prodrug nanoparticle for combination therapy of cancer, Sci. Rep. 6 (2016) 21225.
[18] X. Hejian, Z. Dongfang, Q. Yanxin, Z. Zhiyun, X. Zhigang, C. Xuesi, J. Xiabin, M. Fanbo, H. Yubin, Doxorubicin-loaded carborane-conjugated polymeric nanoparticles as delivery system for combination cancer therapy, Biomacromolecules 16 (2015) 3980–3988.
[19] L.S. Green, D. Jellinek, C. Bell, L.A. Beebe, B.D. Feistner, S.C. Gill, F.M. Jucker, N. Janjic, Nuclease-resistant nucleic acid ligands to vascular permeability factor/vascular endothelial growth factor, Chem. Biol. 2 (1995) 683–695.
[20] J.R. Nicol, D. Dixon, J.A. Coulter, Gold nanoparticle surface functionalization: a necessary requirement in the development of novel nanotherapeutics, Nanomedicine 10 (2015) 1315–1326.
[21] S. Hong, R. Rattan, I.J. Majoros, J.L. Peters, X. Shi, et al., The role of ganglioside GM1 in cellular internalization mechanisms of poly (amidoamine) dendrimers, Bioconjugate Chem. 19 (2009) 1503–1513.
[22] A. Verma, F. Stellacci, Effect of surface properties on nanoparticle–cell interactions, Small 6 (2010) 12–21.
[23] V. Mailä¨nder, K. Landfester, Interaction of nanoparticles with cells, Biomacromolecules 10 (2009) 2379–2400.
[24] P. Nativo, I.A. Prior, M. Brust, Uptake and intracellular fate of surface-modifi ed gold nanoparticles, ACS Nano 2 (2008) 1639–1644.
[25] S. Xiang, H. Tong, Q. Shi, J.C. Fernandes, T. Jin, K. Dai, X. Zhang, Uptake mechanisms of nonviral gene delivery, J. Control. Release 158 (2012) 371–378.
[26] C. Tomuleasa, O. Soritau, A. Orza, M. Dudea, B. Petrushev, O. Mosteanu, S. Susman, A. Florea, E. Pall, M. Aldea, G. Kacso, V. Cristea, I. Berindan-Neagoe, A. Irimie, Gold anoparticles conjugated with cisplatin/doxorubicin/capecitabine lower the chemoresistance of hepatocellular carcinoma-derived cancer cells, J. Gastrointestin Liver Dis. 21 (2012) 187–196.
[27] S. Iram, S. Khan, A.A. Ansary, M. Arshad, S. Siddiqui, E. Ahmad, R.H. Khan, M.S. Khan, Biogenic Terbium oxide nanoparticles as the Vanguard against Osteosarcoma, Spectrochim. Acta Part A 168 (2016) 123–131.
[28] R.Y. Tsang, T. Al-Fayea, H.J. Au, Cisplatin overdose, Drug Saf. 32 (2009) 1109–1122.
[29] G.T. Hermanson, The Definitive Source for Information on Protein Crosslinking, Labeling and Surface Attachment. Bioconjugate Techniques, Academic Press, 1996.
[30] A. Ecaterina, A. Ficai, M.G. Albu, V. Mitran, M. Sonmez, D. Ficai, R. Ion, A. Cimpean, Collagen-hydroxyapatite/cisplatin drug delivery systems for locoregional treatment of bone cancer, Technol. Cancer Res. Treat. 12 (2013) 275–284.
[31] X. Jiang, S. Zhang, A. Machado, S. Lecommandoux, O. Sandre, F. Gu, A. Colin, Controllable microfluidic production of drug-loaded PLGA nanoparticles using partially water-miscible mixed solvent microdroplets as a precursor, Sci. Rep. 7 (2017) 4794.
[32] P. Joshi, S. Chakraborty, S. Dey, V. Shanker, Z.A. Ansari, S.P. Singh, P. Chakrabarti, Binding of chloroquine–conjugated gold nanoparticles with bovine serum albumin, J. Colloid Interface Sci. 355 (2011) 402–409.
[33] B.J. Berne, R. Pecora, Dynamic Light Scattering: With Applications to Chemistry, Biology, and Physics, John Wiley & Sons, Inc., New York, 2000.
[34] L. Rabinovich-Guilatt, P. Couvreur, G. Lambert, D. Goldstein, S. Benita, C. Dubernet, J. Chem. Phys. Lipids 13 (2004) 11–13.
[35] K.S. Kumar, V. Jaikumar, Gold and Iron Oxide nanoparticle-based ethylcellulose nanocapsules for cisplatin drug delivery, Iran. J. Pharm. Res. 10 (2011) 415–424.
[36] S. Kayal, R.V. Ramanujan, Anti-cancer drug loaded iron–gold core-shell nanoparticles (Fe@Au) for magnetic drug targeting, J. Nanosci. Nanotechnol. 10 (2010) 5527–5539.
[37] M. Chang, C.S. Yang, D.M. Huang, Aptamer-conjugated DNA icosahedral nanoparticles as a carrier of Doxorubicin for cancer therapy, ACS Nano 5 (2011) 6156–6163.
[38] K.R. Hande, Clinical applications of anticancer drugs targeted to topoisomerase II, Biochim. Biophys. Acta 1400 (1998) 173–184.
[39] S.M. Cutts, A. Nudelman, A. Rephaeli, D.R. Phillips, The power and potential of doxorubicin-DNA adducts, IUBMB Life 57 (2005) 73–81.
[40] Y. Liu, W. Lu, Recent advances in brain tumor-targeted nano-drug delivery systems, Expert Opin. Drug Deliv. 9 (2012) 671–686.
[41] B. Sumer, J. Gao, Theranostic nanomedicine for cancer, Nanomedicine 3 (2008) 137–140.
[42] B. Petrushev, S. Boca, T. Simon, C. Berce, I. Frinc, D. Dima, et al., Gold nanoparticles enhance the effect of tyrosine kinase inhibitors in acute myeloid leukemia therapy, Int. J. Nanomed. 11 (2016) 641–660.
[43] C. Pautke, M. Schieker, T. Tischer, A. Kolk, P. Neth, W. Mutschler, S. Milz, Characterization of osteosarcoma cell lines MG-63: Saos-2 and U-2 OS in comparison to human osteoblasts, Anticancer Res. 24 (2004) 3743–3748.
[44] N. Tang, W.X. Song, J. Luo, R.C. Haydon, T.C. He, Osteosarcoma development and stem cell differentiation, Clin. Orthop. Relat. Res. 466 (2008) 2114–2130.
[45] X. Luo, J. Chen, W.X. Song, N. Tang, J. Luo, Z.L. Deng, K.A. Sharff, G. He, Y. Bi, B.C. He, Osteogenic BMPs promote tumor growth of human osteosarcomas that harbor differentiation defects, Lab. Invest. 88 (2008) 1264–1277.
[46] T. Nishida, S. Kondo, A. Maeda, S. Kubota, K.M. Lyons, M. Takigawa, CCN family 2/connective tissue growth factor (CCN2/CTGF) regulates the expression of Vegf through Hif-1α expression in a chondrocytic cell line, HCS-2/8, under hypoxic condition, Bone 44 (2009) 24–31.
[47] K. Iwaya, H. Ogawa, M. Kuroda, M. Izumi, T. Ishida, K. Makai, Clin. Exp. Metastasis 6 (2003) 525–529.
[48] F.X. Dieudonné, A. Marion, E. Haÿ, P.J. Marie, D. Modrowski, High Wnt signaling represses the proapoptotic proteoglycan syndecan-2 in osteosarcoma cells, Cancer Res. 70 (2010) 5399–5408.
[49] L.A. Dykman, N.G. Khlebtsov, Gold nanoparticles in Biology and Medicine: recent advances and prospects, Acta Nat. 3 (2) (2011) 34–55.
[50] P. Mukherjee, R. Bhattacharya, N. Bone, Y.K. Lee, C.R. Patra, S. Wang, et al., Potential therapeutic application of gold nanoparticles in B-chronic lymphocytic leukemia (BCLL): enhancing apoptosis, J. Nanobiotechnol. 5 (2007) 4.
[51] P. Mukherjee, R. Bhattacharya, P. Wang, L. Wang, S. Basu, J.A. Nagy, A. Atala, D. Mukhopadhyay, S. Soker S, Antiangiogenic properties of gold anoparticles, Clin. Cancer Res. 11 (2005) 3530–3534.
[52] S. Khan, S.M.D. Rizvi, M. Avaish, M. Arshad, P. Bagga, M.S. Khan, A novel process for size controlled biosynthesis of gold nanoparticles using bromelain, Mater. Lett. 159 (2015) 373–376.
[53] S.J. Taussig, M.M. Yokoyama, A.K. Chinen. Onari, M. Yamakido, Bromelain: a proteoltic enzyme and its clinical application. A review, J. Med. Sci. 24 (1975) 185–193.
[54] N. Kalra, K. Bhui, P. Roy, S. Srivastava, J. George, S. Prasad, Y. Shukla, Regulation of p53: nuclear factor kappaB and cyclooxygenase-2 expression by bromelain through targeting mitogen-activated protein kinase pathway in mouse skin, Toxicol. Appl. Pharmacol. 226 (2008) 30–37.
[55] J. Massague, TGF beta in cancer, Cell 134 (2008) 215–230.
[56] A.H. El-Far, F.A. Badria, H.M. Shaheen, Possible anticancer mechanisms of some *Costus speciosus* active ingredients concerning drug discovery, Curr. Drug Discov. Technol. 13 (2016) 123–143.
[57] B. Juhasz, M. Thirunavukkarasu, R. Pant, L. Zhan, S.V. Penumathsa, E.R. Secor Jr, S. Srivastava, U. Raychaudhuri, V.P. Menon, H. Otani, R.S. Thrall, N. Maulik, Bromelain induces cardioprotection against ischemia-reperfusion injury through Akt/FOXO pathway in rat myocardium, Am. J. Physiol. Heart Circ. Physiol. 294 (2008) H1365–H1370.
[58] L.P. Hale, P.K. Greer, G.D. Sempowski, Bromelain treatment alters leukocyte expression of cell surface molecules involved in cellular adhesion and activation, Clin. Immunol. 104 (2002) 183–190.
[59] L. Kou, J. Sun, Y. Zhai, Z. He, The endocytosis and intracellular fate of nanomedicines:Implication for rational design, Asian J. Pharm. Sci. 8 (2013) 1–10.
[60] A. Benmerah, C. Lamaze, Clathrin-coated Pits: Vive La Diffeírence, Traffic 8 (2007) 970–982.
[61] J. Mercer, A. Helenius, Virus entry by macropinocytosis, Nat. Cell Biol. 11 (2009) 510–520.
[62] B. Wang, L. Zhang, S.C. Bae, S. Granick, Nanoparticle-induced surface reconstruction of phospholipid membranes, Proc. Natl. Acad. Sci. U. S. A. 105 (2008) 18171–18175.
[63] B.D. Chithrani, A.A. Ghazani, W.C. Chan, Determining the size and shape dependence of gold nanoparticle uptake into mammalian cells, Nano Lett. 6 (2006) 662–668.
[64] I.A. Khalil, K. Kogure, H. Akita, H. Harashima, Uptake pathways and subsequent intracellular trafficking in nonviral gene delivery, Pharmacol. Rev. 58 (2006) 32–45.
[65] H. Kasamatsu, A. Nakanishi, How do animal DNA viruses get to the nucleus, Annu. Rev. Microbiol. 52 (1998) 627–686.
[66] S. Mayor, R.E. Pagano, Pathways of clathrin-independent endocytosis, Nat. Rev. Mol. Cell Biol. 8 (2007) 603–612.
[67] L. Pelkmans, D. Puntener, A. Helenius, Local actin polymerization and dynamin recruitment in SV40- induced internalization of caveolae, Science 296 (2002) 535–539.
[68] A. Kumari, S.K. Yadav, Cellular interactions of therapeutically delivered nanoparticles, Expert Opin. Drug Deliv. 8 (2011) 141–151.